*J. Fluid Mech.* (2004), *vol.* 498, *pp.* 227–244.  
DOI: 10.1017/S0022112003006761 Printed in the United Kingdom

# Premelting dynamics in a continuum model of frost heave

By ALAN W. REMPEL[1]†, J. S. WETTLAUFER[1,2] AND M. GRAE WORSTER[3]

[1]Department of Geology and Geophysics, Yale University, New Haven, CT 06520-8109, USA

[2]Department of Physics, Yale University, New Haven, CT 06520-8120, USA

[3]Institute of Theoretical Geophysics, Department of Applied Mathematics and Theoretical Physics, University of Cambridge, Wilberforce Road, Cambridge CB3 0WA, UK

(Received 13 May 2002 and in revised form 23 August 2003)

Frost heave is the process by which the freezing of water-saturated soil causes the deformation and upward thrust of the ground surface. We describe the fundamental interactions between phase change and fluid flow in partially frozen, saturated porous media (soils) that are responsible for frost heave. Water remains only partially frozen in a porous medium at temperatures below 0 °C owing both to the depression of the freezing temperature at curved phase boundaries and to interfacial premelting caused by long-range intermolecular forces. We show that while the former contributes to the geometry of fluid pathways, it is solely the latter effect that generates the forces necessary for frost heave. We develop a simple model describing the formation and evolution of the ice lenses (layers of ice devoid of soil particles) that drive heave, based on integral force balances. We determine conditions under which either (i) a single ice lens propagates with no leading frozen fringe, or (ii) a single, propagating ice lens is separated from unfrozen soil by a partially frozen fringe, or (iii) multiple ice lenses form.

## 1. Introduction

Frost heave is the term given to the upwards displacement of the ground surface caused by the formation of ice within fine-grained soils. It has long been recognized (Taber 1929, 1930) that frost heave requires the flow of unfrozen water towards the freezing front and is unrelated to the fact that water expands upon freezing. Fluids that contract upon freezing also produce heave, as demonstrated first by Taber, who performed experiments on a soil saturated with benzene, and more recently by experiments in which helium (Mizusaki & Hiroi 1995) and argon (Zhu *et al.* 2000) were solidified in porous glass and silica powder respectively.

There has been much uncertainty about the nature of the unfrozen water in porous media, and therefore many suggestions have been made for the mechanism that drives the flow necessary for frost heave. Unfrozen (premelted) water exists at temperatures below the bulk-melting temperature $T_m$ for two reasons: the equilibrium freezing temperature is depressed at a solid–melt interface that has its centre of curvature in the solid; and long-range intermolecular forces (such as van-der-Waals forces or those

† Present address: Division of Engineering and Applied Sciences, Harvard University, 29 Oxford Street, Cambridge, MA 02138, USA.

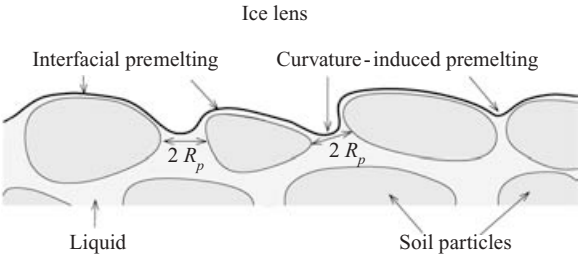


FIGURE 1. A cross-section through the region near the base of a growing ice lens. The characteristic radius of the pore throat, which is half the distance between two adjacent particles, is $R_p$.

that arise from interactions among soluble impurities) between different materials and phases can cause melt to form at free surfaces and at interfaces in contact with another material. For example, ice is known to premelt against its own vapour and against silica (Dash, Fu & Wettlaufer 1995; Wettlaufer 1999*a*) in a layer several nanometres thick at $-1\,^{\circ}\mathrm{C}$ and becoming thicker as the temperature increases towards the bulk melting temperature of $0\,^{\circ}\mathrm{C}$. Figure 1 illustrates how curvature-induced premelting gives rise to supercooled pore water in a porous medium, while interfacial premelting gives rise to unfrozen liquid films separating ice from soil particles.

While pore dimensions are on the scale of microns, the films are on the scale of nanometres. The difficulty of probing materials on such small length scales prompted early modellers of frost heaving to suggest that the water in unfrozen films (variously called quasi-liquid or adsorbed liquid) has strange properties, different from those of bulk water, which cause it to flow down temperature gradients. For example, Vignes-Adler (1977) suggested that the liquid pressure in the films is anisotropic, having a longitudinal tension. Others (e.g. Gilpin 1980) have simply noted the empirical evidence for flow from warmer to colder regions and postulated the existence of a chemical potential gradient that drives a flux of water molecules.

Around the same time that Taber (1929, 1930) first identified the fluid transport associated with frost heave, Beskow (1935) noted the similarity between the unfrozen water content during soil freezing and the residual water saturation encountered during soil drying. This led some (e.g. Everett 1961) to suggest that the water transport during frost heave is akin to capillary rise of water into a dry porous medium, driven by surface tension at the interfaces between ice and pore water. The same idea pervades discussions by O'Neill & Miller (1985) and Fowler (1989, 1997), who suggest that the flow of unfrozen water is a consequence of gradients in pore-water pressure arising from temperature-dependent variations in the curvature of the ice–pore-water interfaces. While this is phenomenologically consistent – the curvature is larger and the pore-water pressure is lower at lower temperatures – we show in this paper that the pore-water pressure is not directly related to the curvature of the ice–water interfaces, and the associated surface energy plays no role in determining the upwards force that causes heave.

The mechanism of frost heave that we quantify is simply that the soil and ice grains repel each other across the interfacially premelted liquid films as a consequence of the same intermolecular forces that give rise to the films (Dash 1989). Low pressure is thus generated in the films, which draws in surrounding water, as into a withdrawn piston. The rate of heaving is mediated by the mobility of the water through the partially frozen soil, i.e. by the permeability of the soil and the viscosity of the water.

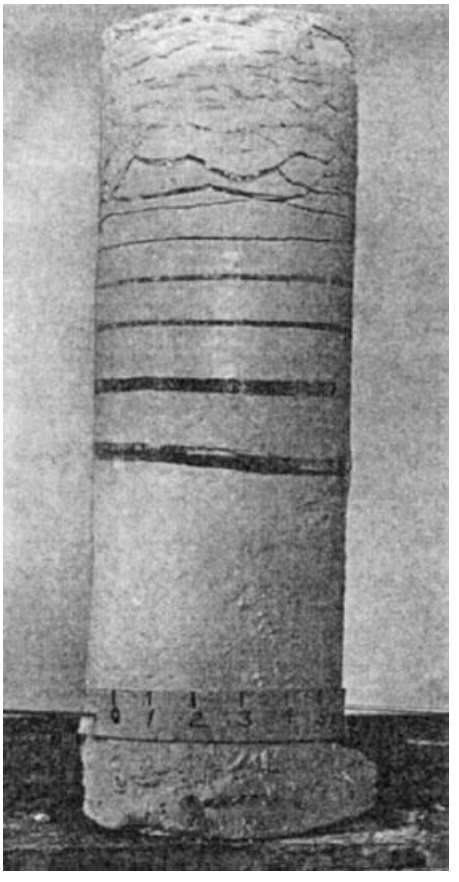

FIGURE 2. A photograph, modified from Taber (1930), showing a series of dark ice lenses that are separated by intervening, lighter layers of partially frozen soil. A cold temperature was applied to the upper surface of the cylindrical clay sample so that solidification proceeded from the top down, with lower lenses growing at later times. The formation of ice lenses caused the sample surface to heave a distance equal to the combined thickness of the lenses. The scale bar at the bottom is in centimetres.

Recent direct measurements using atomic force microscopy (Raviv & Klein 2002) have shown that water behaves as a Newtonian fluid, with no change in its viscosity, down to scales of about two molecular diameters. We therefore work with the assumption that all the unfrozen, supercooled water in a porous medium is Newtonian and seek a quantitative description of frost heaving using classical hydrodynamics, though taking explicit account of the intermolecular forces that give rise to the premelted liquid films. This work builds upon recent studies (Wettlaufer & Worster 1995; Wettlaufer *et al.* 1996) of the flow of liquid in premelted films, which similarly made the assumption that the premelted liquid is Newtonian and obtained predictions in very good agreement with experiments by Wilen & Dash (1995).

Frost heaving often occurs while a series of discrete, soil-free ice lenses form parallel to the isotherms and alternate with layers of soil that contain ice in their pores (figure 2). It is usually assumed that pore ice additionally exists in a 'frozen fringe' separating the warmest (lowermost) ice lens from unfrozen soil. A model of the frozen fringe was proposed by O'Neill & Miller (1985), who introduced a criterion

for the initiation of a new ice lens within the fringe using a prescribed partition of total stress between the ice, soil particles and pore water. In contrast, Worster & Wettlaufer (1999) proposed a model for a single ice lens with no frozen fringe, which is similar to the pushing of a suspended particle in a melt at an advancing solidification front (Chernov, Tempkin & Mel'nikova 1976; Rempel & Worster 1999, 2001). The model in this paper has much in common with the model of O'Neill & Miller (1985) but differs in two important respects: we recognize the need to determine fluid pressures from integral force balances, given that the fluid is bounded by rigid elastic solids (ice and soil particles); and we take explicit account of the microscopic physics that drives the frost-heaving process. In consequence, we are able to replace the prescribed partitioning of total stress with an exact integral expression for the frost-heaving pressure. Moreover, we recognize that although the analogy with wetting characteristics of unfrozen soil can be used to determine the volume fraction occupied by ice, it cannot be used to determine pressures directly. The results of our current model are qualitatively similar to those of O'Neill & Miller (1985) when there is a frozen fringe present, but we additionally predict the conditions under which no frozen fringe exists, when it reduces to the model of Worster & Wettlaufer (1999).

As an introduction to the fluid dynamics and thermodynamics that enable soils to heave, in § 2 we analyse the motion of an isolated particle through a solid such as ice, subjected to a temperature gradient, by a process of melting and refreezing known as thermal regelation. Using the insight thus gained, we develop in § 3 a continuum model to predict the *heave rate* at which an ice lens grows as a function of the temperature at its boundary. We identify a maximum heave rate and consider the dynamics when the *freezing rate* at which the isotherms advance exceeds the heave rate so that the temperature at the lens boundary decreases over time. By examining the conditions that apply beneath the lens boundary, we derive a criterion to predict where a new lens can form and determine the basic characteristics that a soil must possess in order to heave. In § 4 we explore how changes to the control parameters alter the freezing behaviour so that either: (i) no segregated ice lenses will grow, or (ii) a single lens will grow in steady state, or (iii) periodic ice lenses will form. We summarize our findings in § 5 and suggest directions for future work.

## 2. Thermal regelation

If a solid surrounds a substrate particle against which it premelts, as shown in figure 3, then a temperature gradient will cause the particle to move by a process of melting and refreezing known as *thermal regelation.* This phenomenon was first modelled by Gilpin (1979) and discussed in the context of interfacial premelting by Worster & Wettlaufer (1999). We revisit it here in order to illustrate the dominant mechanisms involved in frost heave in a simpler context.

If a particle is separated from the surrounding solid by a thin layer of liquid then the total surface energy of the solid–melt and melt–particle interfaces is less than the surface energy of a solid–particle interface. Such is the case for the system ice–water–silica, for example. The net intermolecular forces between the solid, the premelted liquid film and the particle are then such as to repel the particle from the ice with a force per unit area, $p_T(d)$ that depends on the film thickness $d$. In the wetting literature, $p_T(d)$ is referred to as the *disjoining pressure* (e.g. de Gennes 1985; Schick 1990). Minimization of the total free energy of the system gives the equilibrium

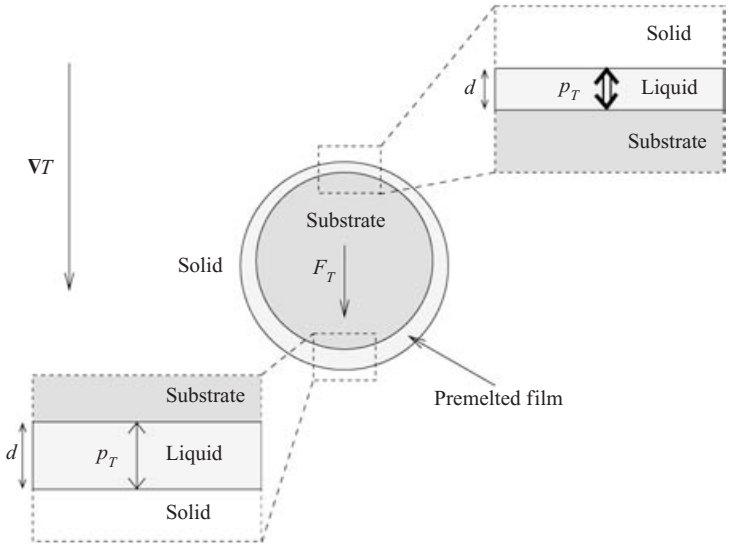


FIGURE 3. A schematic diagram of a substrate that is separated from a solid by a premelted film and held within a temperature gradient $\nabla T$. The film thickness $d$ is thinner on the cold side of the substrate than on its warm side, and hence the repulsive pressure between the substrate and the solid $P_T$ is spatially varying. This gives rise to a net thermomolecular force $\boldsymbol{F}_T$ that tends to push the substrate towards warmer temperatures.

condition

$$\rho_s L \frac{T_m - T}{T_m} = \gamma_{sl}\mathscr{K} + p_T(d) \tag{2.1}$$

(e.g. Baker & Dash 1989; Rempel & Worster 2001) where $\rho_s$ is the density of the solid (ice), $L$ is the latent heat of fusion per unit mass, and $\gamma_{sl}$ is the surface energy of the solid–liquid interface, which has a curvature $\mathscr{K}$ that is defined to be positive when the centre of curvature is in the solid. The right-hand side of equation (2.1) describes the interfacial effects that enable liquid to remain in equilibrium within the solid region of the bulk-phase diagram. In the absence of these interfacial effects, bulk thermodynamics tells us that liquid and solid can only coexist at equilibrium when the temperature $T = T_m$. The left-hand side of equation (2.1) quantifies the degree of departure from bulk coexistence that is associated with these interfacial effects. We note that, more generally, $T_m$ also depends on pressure so that a second term, related to the Clausius–Clapeyron slope, can be incorporated on the left-hand side; the magnitude of this effect is negligible and does not play a significant role in the dynamics of the current problem (see e.g. equation (2.7) of Dash *et al.* 1995).

The reduction in $p_T$ with increasing film thickness $d$ is controlled by the type and strength of the intermolecular interactions that dominate the system. With non-retarded van-der-Waals forces, for example,

$$p_T = \mathscr{A}/6\pi d^3, \tag{2.2}$$

where $\mathscr{A}$ is the total effective Hamaker constant. In the cases that we treat here, the substrate dimensions are much larger than the film thickness, so the interfacial curvature is dictated by the substrate geometry. A temperature decrease is accommodated by a reduction in film thickness. For reference, the premelted film separating ice from a planar (i.e. $\mathscr{K} = 0$) substrate is typically of order $10^{-8}$ m thick

when the temperature is a few tenths of a degree below $T_m$ (e.g. see, most recently, figure 1 of Sadtchenko & Ewing 2002) and diverges as the temperature warms to $T_m$.

The net *thermomolecular force* on the particle, arising from the intermolecular interactions, is

$$\boldsymbol{F}_T \equiv -\int_\Gamma p_T \,\mathrm{d}\Gamma = \int_\Gamma \left(\gamma_{sl}\mathscr{K} - \rho_s L\frac{T_m - T}{T_m}\right)\mathrm{d}\Gamma \tag{2.3}$$

where the surface area element $\mathrm{d}\Gamma$ points in the direction of the outward normal to the particle. An important result is that the integral of the curvature term is zero (Rempel, Wettlaufer & Worster 2001), so that

$$\boldsymbol{F}_T = \frac{\rho_s L}{T_m}\int_{\mathscr{D}} \nabla T \,\mathrm{d}V, \tag{2.4}$$

where $\mathscr{D}$ is the interior of $\Gamma$, as can be seen by applying the divergence theorem to the final integral in (2.3). Equation (2.4) can be written as

$$\boldsymbol{F}_T = m_s\frac{L}{T_m}\langle\nabla T\rangle = m_s\boldsymbol{G} \tag{2.5}$$

where $\langle\nabla T\rangle$ is the mean of the temperature gradient over the interior of the particle, $m_s$ is the mass of solid displaced by the particle and $\boldsymbol{G}\equiv(L/T_m)\langle\nabla T\rangle$. If the particle and surrounding solid have different thermal conductivities then the mean internal temperature gradient may be a function of the conductivity ratio and the geometry of the particle. However, in this paper we ignore those complications, which are not fundamental to the frost-heaving mechanism, by taking the conductivities to be equal, in which case $\boldsymbol{G}=(L/T_m)\nabla T$, where $\nabla T$ is the applied temperature gradient. The importance of the simple result (2.5) is that the net thermomolecular force is independent of the curvature and independent of the type and strength of the intermolecular interactions giving rise to $p_T$. Furthermore, the net force is simply proportional to the mass of displaced solid (ice), which is a key feature of the model of frost heave to be introduced.

In order for the particle to move (for heave to occur) given the force $\boldsymbol{F}_T$, the premelted liquid in the thin film surrounding the particle must flow from fore (warm) to aft (cold). Here the geometry and thickness of the film, influenced both by curvature and by the intermolecular interactions, play a crucial role in determining flow rates.

For illustrative purposes, consider a spherical particle of radius $R$ that is much greater than the thickness of the premelted film. We neglect the density difference between water and ice, in which case mass conservation implies that the volume flux of fluid integrated over the azimuthal angle is

$$q = -\pi(R\sin\theta)^2 U \tag{2.6}$$

where $U$ is the speed of the particle in the opposite direction and $\theta$ is the polar angle. Lubrication theory (Batchelor 1967) is used to express the volume flux in terms of the pressure gradient as

$$q = \frac{\pi d^3\sin\theta}{6\mu}\frac{\mathrm{d}p_l}{\mathrm{d}\theta}, \tag{2.7}$$

where $d$ is determined from the temperature field via (2.1). For a similar problem, Fowler (1997, p. 367) writes (translating to the notation we use in this paper)

$$p_l = p_i - p_T - \gamma_{sl}\mathscr{K} \tag{2.8}$$

and takes the pressure in the ice $p_i$ to be constant in order to evaluate (2.7) directly – an approach similar to that used in the context of thin-film flows with stress-free surfaces. However, it is important to recognize that, on the time scales relevant to frost heave ice behaves as an elastic solid and can support gradients in normal stress. Therefore, the liquid pressure can only be determined by an integral force balance, similar to the approach needed in squeeze films or slider bearings (e.g. Batchelor 1967): the ice pressure $p_i$ cannot be assumed constant. Combining equation (2.6) with (2.7) and integrating twice, we obtain the net hydrodynamic force on the particle

$$\boldsymbol{F}_\mu = \int_\Gamma p_l \,\mathrm{d}\boldsymbol{\Gamma} = 2\pi R^2 \hat{\boldsymbol{z}} \int_0^\pi p_l \cos\theta \sin\theta \,\mathrm{d}\theta = -\frac{8\pi\mu R^4}{d_0^3}\boldsymbol{U}, \tag{2.9}$$

where $d_0$ is the film thickness at the equator of the particle, where $\theta = \pi/2$. This result can be written as

$$\boldsymbol{F}_\mu = -\frac{4}{3}\pi R^3 \frac{\mu \boldsymbol{U}}{k}, \tag{2.10}$$

in order to make an analogy with the flow in partially frozen soils later, where the permeability

$$k = \frac{d_0^3}{6R} = \frac{\mathscr{A}}{36\pi R}\left[\rho L\left(\frac{T_m - T_0}{T_m}\right) + \frac{2\gamma_{sl}}{R}\right]^{-1} \tag{2.11}$$

depends both on the strength and type of the intermolecular interactions, and on curvature. For illustration, the final expression in (2.11) is obtained using (2.1) for the special case of non-retarded van-der-Waals interactions (2.2).

The net force on the particle is zero, so the sum of $\boldsymbol{F}_T$ and $\boldsymbol{F}_\mu$ must balance the force due to gravity to give

$$\boldsymbol{U} = \frac{\rho d_0^3}{6\mu R}(\boldsymbol{G} + \boldsymbol{g}'), \tag{2.12}$$

where $\boldsymbol{g}' = \boldsymbol{g}(\rho_p - \rho)/\rho$ is the reduced gravity for a particle of density $\rho_p$. For temperature gradients and particle densities that are typical of those found in nature, the effect of gravity is often negligible in comparison to that of the thermomolecular force (i.e. $|\boldsymbol{g}'| \ll |\boldsymbol{G}|$). A micron-sized particle separated from ice by a premelted film of thickness $10^{-8}$ m and experiencing a temperature gradient of $1\,\mathrm{K\,m^{-1}}$ moves by thermal regelation approximately 10 microns per day.

## 3. Frost heave

The physical interactions described above that drive thermal regelation also control the dynamics of frost heave. In both cases the equilibrium condition (2.1) determines the geometry of the fluid pathways (hence the permeability), while the forces produced by intermolecular interactions and gravity are balanced by the hydrodynamic pressure gradient established by the flow.

We examine the one-dimensional system sketched in figure 4, which relates to controlled laboratory experiments (e.g. Mutou *et al.* 1998; Watanabe & Mizoguchi 2000) in which a saturated soil is pulled through an imposed, constant temperature gradient $\nabla T$ at a constant speed $V$. The coordinate frame is fixed relative to the isotherms, with the origin $z = 0$ at temperature $T_m$, and $z$ increasing towards lower temperatures. Since the pulling speed equals the rate at which the 0 °C isotherm advances relative to the soil particles, we refer to $V$ as the freezing rate.

There are potentially three regions: an ice lens in $z > z_l$, which has no soil particles; a frozen fringe in $z_f < z < z_l$ containing soil particles and partially frozen pores; and

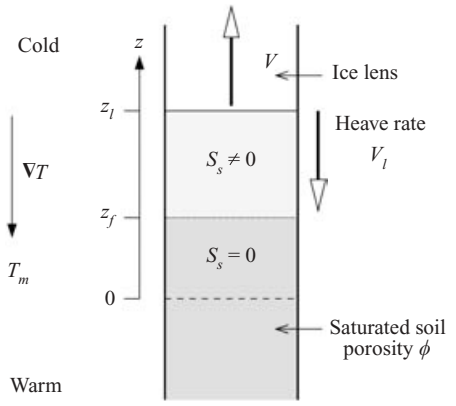


FIGURE 4. A schematic diagram of an ice lens that is pulled through a temperature gradient at a constant speed or freezing rate $V$ and experiences heave rate $V_l$. The porosity $\phi$ in the soil is constant and the fraction of the pore volume that is filled with ice $S_s$ decreases monotonically from the lens boundary $z_l$ to zero at $z_f$.

liquid-saturated, ice-free soil in $z < z_f$. Pore ice can only penetrate the soil where the curvature of the ice–water interface $\mathscr{K} = (\rho_s L/\gamma_{sl})(T_m - T)/T_m$ is greater than $2/R_p$, where $R_p$ is the characteristic radius of the 'throats' between pores. Therefore

$$z_f = \frac{2\gamma_{sl}}{\rho G R_p}, \tag{3.1}$$

where $G \equiv (L/T_m)|\nabla T|$ is constant. For physical intuition, if the pore throats are a micron in diameter then the temperature at $z_f$ is approximately $-0.1\,^{\circ}\mathrm{C}$. If $z_l < z_f$ then no frozen fringe can exist. In this case, there are just two regions: an ice lens in $z > z_l$ and unfrozen soil in $z < z_l$. In either case, the only geometrical variable to be determined is the location $z_l$ of the base of the ice lens. The heave rate $V_l$ is defined as the velocity of the ice lens relative to the soil particles. Thus the position of the lens boundary satisfies

$$\frac{\mathrm{d}z_l}{\mathrm{d}t} = V - V_l(t), \tag{3.2}$$

so that steady states are achieved when $V_l = V$ and the lens boundary migrates towards colder temperatures when $V_l < V$.

Within the frozen fringe, when it exists, there is a fraction $S_s$ (called the ice saturation) of the porosity or pore volume fraction $\phi$ that is occupied by ice. Assuming local equilibrium, $S_s$ is a function of the geometry of the soil particles, the packing arrangement, and the local temperature and pressure. A particular example is given in the Appendix, where we assume constant porosity $\phi$, uniform soil properties and note that the effect of pressure is negligible. Since we are considering a situation in which the temperature is a fixed function of $z$, it follows that $S_s = S_s(z)$ only.

### 3.1. *Lens growth*

The intermolecular interactions between the soil particles and the ice produce the net force

$$\boldsymbol{F}_T \equiv -\int_\Gamma p_T \,\mathrm{d}\Gamma = \int_\Gamma (\gamma_{sl}\mathscr{K} - \rho G z)\,\mathrm{d}\Gamma \tag{3.3}$$

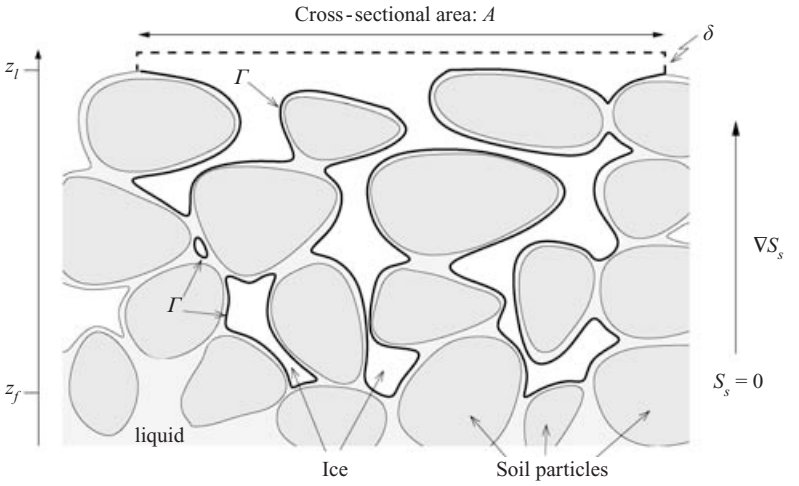


FIGURE 5. A cross-section through the region near the base of an ice lens. Ice extends into the pore space beneath the lens boundary at $z_l$ and forms a connected, three-dimensional network with its surface $\Gamma$ separated from the soil particles by premelted liquid. The position $z_f$ marks the temperature at which the effects of interfacial curvature prevent ice from extending through the pore throats into the adjacent, warmer pores.

that causes heave, where $\Gamma$ is the entire surface of the ice connected to the lens and $\mathrm{d}\Gamma$ points in the direction of the outward normal to the ice. The surface $\Gamma$ can be closed by the addition of the dashed surface shown in figure 5, and the divergence theorem applied to show that the force on a cross-section of the lens of area $A$ is

$$\boldsymbol{F}_T = \rho A G\,\hat{\boldsymbol{z}} \int_0^{z_l} (1 - \phi S_s)\,\mathrm{d}z. \tag{3.4}$$

Just as in the case of the regelating sphere analysed in § 2, the curvature term integrates to zero and the resultant force is proportional to the volume of the region that is cooler than the bulk melting temperature, but does not contain ice.

Equation (3.4) replaces the temperature-dependent term in equation (25) of O'Neill & Miller (1985), which in our notation can be written

$$\boldsymbol{F}_T^{OM} = \rho A G z_l\,\hat{\boldsymbol{z}}, \tag{3.5}$$

i.e. the second term in the integrand of (3.4) is missing. More important than the quantitative difference produced is the physical understanding of the origin of $\boldsymbol{F}_T$ that we have given, which can be carried over to other problems. The false physical reasoning that leads to (3.5) is that the pressure in the ice is locally uniform (cf. the discussion surrounding equation (2.8)), whereas large variations in the stress within the ice can persist over the time scales during which liquid is supplied to the growing lens. Once the ice pressure is assumed to be locally uniform then it can be calculated as being equal to the pore-water pressure minus the surface energy times the curvature of the ice–water interface, and the false dynamic analogy with capillary wetting of dry soils is advanced.

In order for the force calculated by equation (3.4) to cause heave, continuity demands that water is drawn through the pores to the lens and fringe. The resultant

low pressure in the water produces a net hydrodynamic force on the lens given by

$$\boldsymbol{F}_\mu = -\int_\Gamma p_l \, \mathrm{d}\Gamma, \tag{3.6}$$

where $p_l$ is the deviation in the fluid pressure from hydrostatic equilibrium. Applying the divergence theorem, we obtain the hydrodynamic force on a segment of the lens surface with cross-sectional area $A$ as

$$\boldsymbol{F}_\mu = A\int_{z_h}^{z_l} \nabla p_l \, (1-\phi S_s)\, \mathrm{d}z = -A\int_{z_h}^{z_l} \frac{\mu \boldsymbol{U}}{k}\,(1-\phi S_s)\, \mathrm{d}z, \tag{3.7}$$

where $k(S_s)$ is the permeability and $z_h$ is the position at which the fluid pressure attains hydrostatic equilibrium, so that $p_l(z_h)=0$. This expression can be compared with equation (2.9). Continuity relates the transport velocity to the heave rate so that $\boldsymbol{U}=(1-\phi S_s)V_l\,\hat{\boldsymbol{z}}$ and equation (3.7) can be written as

$$\boldsymbol{F}_\mu = -\mu V_l A\,\hat{\boldsymbol{z}}\int_{z_h}^{z_l} \frac{(1-\phi S_s)^2}{k}\,\mathrm{d}z. \tag{3.8}$$

Note that the hydrodynamic force on the lens surface is proportional to the heave rate and increases, for a given heave rate, as increased ice saturation reduces the permeability.

The net force on the lens boundary is zero, so the sum of $\boldsymbol{F}_T$ and $\boldsymbol{F}_\mu$ must balance the force of gravity on the overlying material $\boldsymbol{F}_O = -P_O A\,\hat{\boldsymbol{z}}$, where the overburden pressure $P_O$ is treated as a constant. Combining this with equations (3.4) and (3.8), we find that the heave rate is

$$V_l = \left[\rho G\int_0^{z_l}(1-\phi S_s)\,\mathrm{d}z - P_O\right]\left[\mu\int_{z_h}^{z_l}\frac{(1-\phi S_s)^2}{k}\,\mathrm{d}z\right]^{-1}. \tag{3.9}$$

This expression, used in (3.2), determines the evolution of the ice lens once the ice saturation is determined from thermodynamic considerations. Note that the predictions from equation (3.9) are not sensitive to the value of $z_h$ as long as most of the drop in hydrodynamic pressure occurs near the lens boundary, where the permeability is reduced by the confining presence of ice.

There are some aspects of the system that are similar no matter what the precise spatial distributions of $S_s$ and $k$. For example, the heave rate is zero when the thermomolecular force balances the overburden, which occurs when

$$P_O = P_{max} \equiv \rho G\int_0^{z_l}(1-\phi S_s)\,\mathrm{d}z. \tag{3.10}$$

$P_{max}$ is referred to as the *maximum frost-heave pressure*. The intermolecular interactions between the lens and the soil particles are insufficient to support loads that are greater than $P_{max}$ – these cause the lens to melt rather than grow. For physical intuition, $P_{max}$ is approximately one atmosphere (0.1 MPa) when the temperature at the lens boundary is $-0.1\,^\circ$C. When no frozen fringe is present, $S_s=0$ and $P_{max}=\rho G z_l$ is equivalent to the maximum crystallization pressure discussed by Derjaguin & Churaev (1978) and is consistent with the predictions of O'Neill & Miller (1985). However, equation (3.10) shows that once a frozen fringe is present $P_{max} < \rho G z_l$.

The lens grows ($V_l > 0$) when the overburden is less than $P_{max}$. The heave rate is then given as a function of the position $z_l$ of the base of the ice lens by a curve similar to that shown in figure 6. The figure is plotted in terms of dimensionless variables,

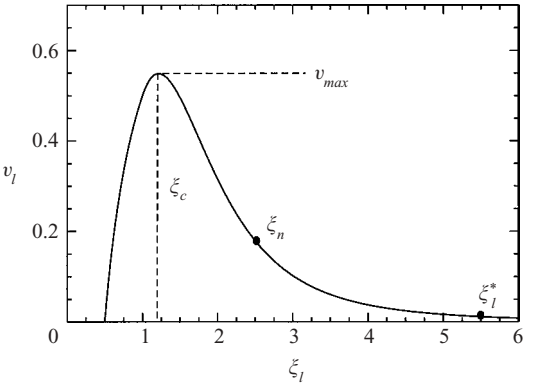


FIGURE 6. The heave rate of an ice lens as a function of its boundary position for the ice saturation and permeability models that are described in the Appendix, calculated using $p_o = 0.5$, $\phi = 0.5$ and $\xi_h = 0$ in equation (3.11). For a temperature gradient of $1\,^{\circ}\mathrm{C\,m^{-1}}$, when the radii of the pore throats are approximately $10^{-6}$ m so that the temperature at the fringe boundary is $-0.1\,^{\circ}$C, a dimensionless position of unity corresponds to a distance from the $T_m$ isotherm of 0.1 m. A typical ice-free permeability for such a fine-grained soil is $k_0 \approx 10^{-14}$ m$^2$, which would indicate that a dimensionless heave rate of unity corresponds to approximately $10^{-5}\,\mathrm{m\,s^{-1}}$. The points $\xi_n$ and $\xi_l^*$ are discussed in § 3.2.

$\xi_l \equiv z_l/z_f$ and

$$v_l \equiv \frac{\mu V_l}{k_0 \rho G} = \left[\int_0^{\xi_l} (1 - \phi S_s)\,\mathrm{d}\xi - p_o\right]\left[\int_{\xi_h}^{\xi_l} \frac{(1-\phi S_s)^2}{\tilde{k}}\,\mathrm{d}\xi\right]^{-1}, \qquad (3.11)$$

where $\xi \equiv z/z_f$, $\xi_h \equiv z_h/z_f$, $p_o \equiv P_O/(\rho G z_f)$, $\tilde{k}(\xi) \equiv k/k_0 \geqslant 1$ and $k_0$ is the permeability of the ice-free soil. For $\xi < 1$, $S_s = 0$ and $\tilde{k} = 1$. Figure 6 was produced using the specific models for ice saturation $S_s(\xi \geqslant 1) = 1 - \xi^{-2}$ and permeability $\tilde{k}(\xi \geqslant 1) = \xi^{-4}$ described in the Appendix and given by equations (A 1) and (A 2) respectively. However, the qualitative aspects of figure 6 are universal. Note first that since $S_s \to 1$ and the permeability $k(S_s)$ thus tends to zero as $z \to \infty$, equation (3.9) implies that the heave rate $V_l$ tends to zero at large values of $z_l$. Therefore, since $V_l$ is zero when the lens boundary is located where $P_O = P_{max}$ and is positive at larger values of $z_l$, there is always a maximum heave rate $V_{max}$ attained at an intermediate position of the lens boundary. The same qualitative behaviour is also predicted when the frozen fringe is not present (Worster & Wettlaufer 1999).

When the freezing rate $V$ is less than $V_{max}$, a steady state can develop with the lens boundary at the fixed position where $V_l = V$. The curve in figure 6 would seem to indicate that two steady-state lens positions are possible for any particular $V < V_{max}$. However, further analysis shows that only the branch of the curve with $\xi_l < \xi_c$ is stable to perturbations of the boundary position – a point we return to later. At colder temperatures where $\xi_l > \xi_c$ the reduction in permeability associated with further increases in ice saturation causes the heave rate to decrease with $\xi_l$. Hence, the temperature at the lens boundary decreases as the heave rate continues to trace the curve in figure 6 and an increasing fraction of the pore space fills with ice. This suggests the potential for a new lens to form at a location where the temperature is higher.

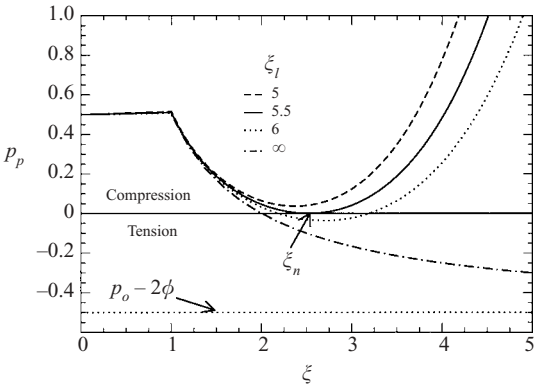


FIGURE 7. The scaled pressure between soil particles as a function of position for $p_o = 0.5$, $\phi = 0.5$ and $\xi_h = 0$ using the ice saturation and permeability relations described by equations (A 1) and (A 2). Each line represents the profile obtained when the lens boundary is at a different position $\xi_l$, as noted in the legend. The soil particles are pushed against each other when $p_p > 0$, whereas they are pulled apart when $p_p < 0$; there is no net force between the soil particles at $\xi_n$. The horizontal dotted line at $p_p = p_o - 2\phi$ shows the asymptote as $\xi \to \infty$ for the curve corresponding to $\xi_l \to \infty$.

### 3.2. *Lens initiation*

To determine where a new lens can form, we consider the net vertical force $\boldsymbol{F}_p$ acting between soil particles. At a position $z < z_l$ within the frozen fringe the net thermomolecular and hydrodynamic forces on the ice are given by expressions similar to (3.4) and (3.8) respectively with the upper limits of integration $z_l$ replaced by $z$. Therefore, since $\boldsymbol{F}_p$ balances the sum of $\boldsymbol{F}_T$, $\boldsymbol{F}_\mu$ and $\boldsymbol{F}_O$, we have

$$\boldsymbol{F}_p = \mu V_l A \hat{\boldsymbol{z}} \int_{z_h}^{z} \frac{(1-\phi S_s)^2}{k}\,\mathrm{d}\eta + P_O A \hat{\boldsymbol{z}} - \rho G A \hat{\boldsymbol{z}} \left( z\phi S_s - \int_0^z \phi S_s\,\mathrm{d}\eta \right), \tag{3.12}$$

which can be written in dimensionless form as

$$p_p \equiv \frac{\boldsymbol{F}_p \cdot \hat{\boldsymbol{z}}}{\rho G z_f A} = v_l \left[ 1 - \xi_h + \int_1^{\xi} \frac{(1-\phi S_s)^2}{\tilde{k}}\,\mathrm{d}\eta \right] + p_o - \left( \xi\phi S_s - \int_1^{\xi} \phi S_s\,\mathrm{d}\eta \right), \tag{3.13}$$

with $v_l$ determined from equation (3.11). Note that the final bracketed term in (3.12) reduces to (3.4) when $z = z_l$, where the total ice fraction $\phi S_s = 1$.

A new lens can form at the position $z_n$ where $\boldsymbol{F}_p = 0$ and there is no net force to hold the particles together. Equation (3.12), or equivalently (3.13), provides a general expression that accounts for the effects of the microphysical interactions between the soil particles, the ice and the premelted liquid. It depends only on physical properties, such as $\rho$ and $\mu$, control parameters, such as $G$ and $P_O$, and characteristics of the soil that can, in principle, be measured, namely $\phi$, $S_s$ and $k$. We use equation (3.12) in our model to provide a prediction of the conditions required to form a new lens, thus avoiding the need to prescribe a stress-partition function, such as that used by O'Neill & Miller (1985).

In figure 7 we plot the scaled pressure between soil particles $p_p$ as a function of the dimensionless position, using the ice saturation and permeability models described in the Appendix. Separate profiles are displayed for the different locations of the lens boundary noted in the legend. In the liquid-saturated soil beneath $\xi = 1$ the force between soil particles balances the combination of the overburden and

the hydrodynamic force associated with fluid flow. Once $\xi > 1$, a thermomolecular force pushes against the pore ice and transmits a portion of the load to the lens so that initially the net vertical force between soil particles decreases with $\xi$. The resistance to fluid flow is enhanced with increased ice saturation, and at some point the rising hydrodynamic force overcomes further increases in the thermomolecular force so that the net pressure between soil particles begins to increase with $\xi$. When $\xi_l > \xi_c$ and the lens is brought to a colder temperature, the flow velocity decreases and the net force between soil particles can vanish at some level $\xi_n \equiv z_n/z_f$, as shown by the solid curve in figure 7 for $\xi_l \equiv \xi_l^* \approx 5.5$. In the example given here we expect a new lens to form at $\xi_n \approx 2.5$, and the dimensionless lens spacing is predicted to be $\xi_l^* - \xi_n \approx 3$.

It is observed that clays, silts and other fine-grained porous media heave, whereas coarse sands and gravels do not. For an ice lens to form at all, so that heave can occur, a minimum requirement is that the thermomolecular force exerted by the pore ice must support the overburden. In the limit that $\xi_l$ tends to infinity, the heave rate tends to zero and equation (3.13) shows that the pressure between soil particles approaches

$$p_p = p_o - \phi \left[ \xi S_s - \int_1^{\xi} S_s \, \mathrm{d}\eta \right]. \tag{3.14}$$

For example, using the ice saturation model from equation (A 1) we find that

$$p_p = p_o - 2\phi \left( 1 - \frac{1}{\xi} \right), \tag{3.15}$$

which is displayed with the dot-dashed line in figure 7. Clearly, with this ice saturation model a new lens can only form if $p_o < 2\phi$. This is equivalent to stating that new lenses can only form when the fringe boundary is sufficiently cold that

$$z_f \geqslant \frac{P_O}{2\phi\rho G}. \tag{3.16}$$

From the definition of $z_f$ in equation (3.1), this implies that the radii of the pore throats is limited by

$$R_p \leqslant \frac{4\phi\gamma_{sl}}{P_O}. \tag{3.17}$$

This places a constraint on the characteristics that a soil must possess in order to be susceptible to significant heave. For example, if the porosity is 0.5 and the overburden to be heaved is equivalent to the weight of a layer of soil one centimetre thick so that $P_O \approx 10^2$ Pa, then the soil is only 'frost susceptible' if the pore throats are less than about $10^{-3}$ m in radius.

## 4. Discussion

The various predictions of the model presented above are summarized in the regime diagram presented in figure 8, which shows the predicted behaviour given values of the control parameters $V$ and $P_O$. The solid lines separate three main regions corresponding to having a steady lens without a frozen fringe, periodic ice lenses or no segregated ice. The solid line

$$v = 1 - p_o \tag{4.1}$$

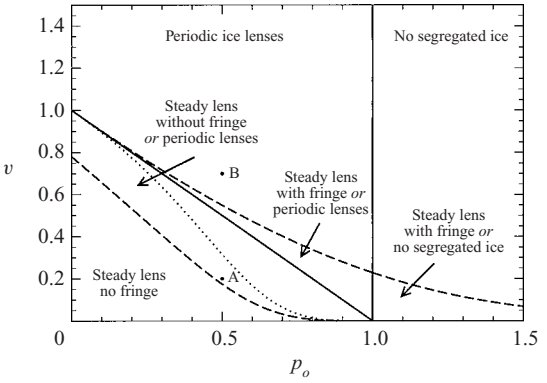


FIGURE 8. A regime diagram displaying the behaviour as a function of the freezing rate $v$ and overburden $p_o$. At low $v$ and $p_o$, a steady lens will grow without a frozen fringe. At higher $v$, periodic ice lenses will form. At higher $p_o$ ($p_o > 1$ for $\phi = 0.5$), no segregated ice lenses can be inititated. Hysteretic behaviour is possible at intermediate $v$ and $p_o$, as described in the text. Points A and B are discussed in figure 9.

corresponds to the condition that $\xi_l = 1$, as can be seen from equation (3.11). For lower freezing rates it is possible to have a steady lens with no frozen fringe. Starting from such a state, the lens boundary can only penetrate the pores to form a frozen fringe once $z_l > z_f$ (i.e. $\xi_l = 1$), which is a necessary precursor for periodic lensing, as we have seen. The vertical solid line at $p_o = 2\phi$ indicates the overburden pressure above which it is possible to have no segregated ice, as was described at the end of the last section. More generally, for different ice saturation models, this regime boundary is found where equation (3.14) is satisfied for $p_p = 0$ in the asymptotic limit $\xi \to \infty$.

However, the system is hysteretic. If the freezing rate $v$ is increased from zero and $p_o < 2\phi$ then a steady lens with no fringe gives way to a steady lens with a fringe, which becomes unsteady and produces periodic lenses once $v$ exceeds $v_{max}$, indicated by the upper dashed curve. If the freezing rate is subsequently reduced then periodic lensing continues until $v < v_l(\xi_n)$, indicated by the lower dashed curve. If $p_o > 2\phi$ and there is a pre-existing lens then it is possible to maintain it propagating steadily with a frozen fringe if $v < v_{max}$. However, if the freezing rate is increased above $v_{max}$ then the lens boundary will recede to infinity without a new lens being initiated. An example of hysteretic behaviour in a case with $p_o < 2\phi$ is shown in figure 9.

The description of the regime diagram thus far has referred to long-term asymptotic states. When $p_o < 2\phi$, and segregated ice is not present initially so that $v_l = 0$, the first lens is formed at the position where the pressure between soil particles, described by equation (3.14), first reaches 0. The dotted line shows the position where the freezing rate matches the initial heave rate of this first lens. Above the dotted line, periodic lensing results; below the dotted line the lens propagates steadily.

The evolving conditions that held during the step-freezing experiment that produced the periodic lensing behaviour shown in figure 2 could be represented on the regime diagram as a progressively decreasing freezing rate at constant overburden. In agreement with the model calculations shown in figure 9, during periodic lensing a reduction in $v$ leads to increased lens thickness. The gradual increase in spacing between the lower lenses shown in figure 2 is consistent with the slow increase in the length scale $z_f$ associated with a reduction in $G$ as freezing progressed.

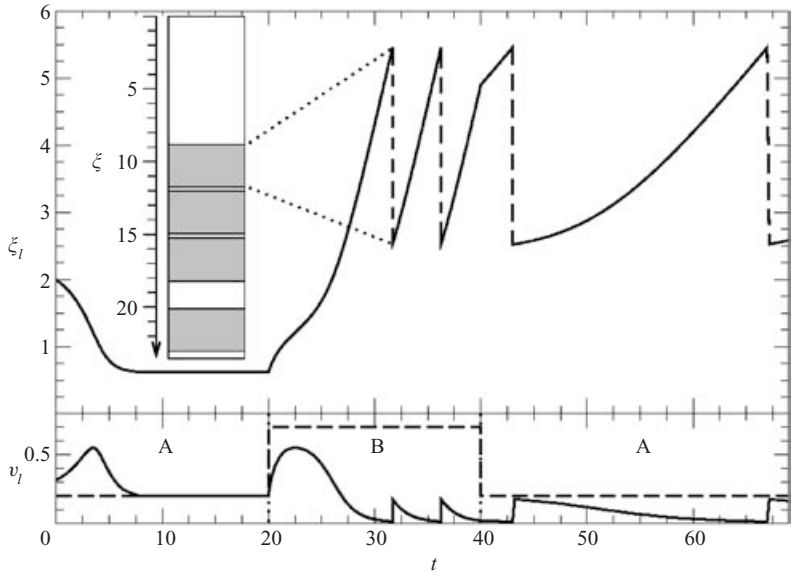


FIGURE 9. The lens position $\xi_l$ and heave rate $v_l$ as a function of time $t$ for a constant load of $p_o = 0.5$. The freezing rate, shown with the dashed line in the lower panel, is set to $v = 0.2$ initially, which corresponds to point A in figure 8. The liquid flow rate is initially zero and the first lens forms at $\xi_l = 2$, as marked by the $\xi$-intercept of the curve for $\xi_l \to \infty$ in figure 7. Since $v < v_l(\xi_l = 2)$ (i.e. point A is below the dotted line in figure 8), the lens grows towards warmer temperatures and approaches a steady state with $v_l = v$, as shown by the solid line in the lower panel. At $t = 20$, $v$ is increased to 0.7, corresponding to point B in figure 8, so that $v > v_{max}$ (i.e. point B is above the upper dashed line in figure 8). The lens recedes to colder temperatures and a new lens is initiated at $\xi_n \approx 2.5$ when $\xi_l = \xi_l^* \approx 5.5$. The new lens then grows as it recedes to $\xi_l^*$ and the sequence repeats. At $t = 40$, $v$ is reduced to 0.2 once again. Periodic lens growth continues since $v > v_l(\xi_l \geqslant \xi_n)$ (i.e. point A is above the lower dashed line in figure 8). The inset shows the lens thicknesses $\int v_l dt$ (white) and spacing $\xi_l^* - \xi_n$ (shaded) for this freezing scenario. When the system experiences periodic lens growth, the lenses have more time to grow at smaller $v$ and become thicker. The dimensionless lens spacing is independent of $v$.

## 5. Conclusions

The existence of unfrozen water at the interfaces between soil particles and ice underlies the phenomenon of frost heave in porous media. Our model predicts the macroscopic features (e.g. the heave rate, lens thickness and lens spacing) of the heaving system while taking explicit account of the local intermolecular interactions that drive the entire process. By considering the force balance over the surface of a single soil particle that is coated with premelted liquid and encapsulated in ice, we have shown how the intermolecular interactions acting across the liquid film cause the particle to be pushed towards warmer temperatures, while continuity demands that the premelted liquid flow in the opposite direction. In porous media the same fundamental physics results in the flow of liquid that supplies the lens growth and produces heave. The balances of mass and force over the lens surface determine the heave rate as a function of the thermal conditions on its boundary. Our model explicitly accounts for the microphysical interactions that occur between the soil particles, the ice and the liquid, and yields predictions that are in agreement with observations. When the freezing rate is greater than the heave rate at which a lens grows, its boundary recedes to colder temperatures. For a banded structure to develop, in which ice lenses alternate with layers of soil, the pore space beneath the boundary of the growing

lens must be partially filled with ice. Intermolecular interactions between this pore ice and the soil particles can give rise to a net thermomolecular force that is sufficient to support the combined effects of overburden and hydrodynamic forces. We provide a rigorous justification for the form of the stress-partition relationship, equation (3.12), that determines when the pressure between soil particles vanishes and a new lens can form. This obviates the need for a prescribed stess-partition relationship, which has been a feature of earlier, phenomenological models (e.g. O'Neill & Miller 1985) that neglect essential elements of the microscopic physics. There is a limit to the load that a given soil can heave, and this limit increases as the throats that join adjacent pores decrease in size. The model provides the underlying fluid-mechanical explanation of the qualitative distinctions between the heaving characteristics of various soil types. If the freezing rate drops below the rate at which a newly initiated lens can grow, the lens boundary migrates towards warmer temperatures and a stable steady state can develop in which a single lens grows indefinitely.

To focus on the essential physical interactions that control heaving behaviour we have employed a few simplifying assumptions in constructing our theoretical model. For example, by treating the porosity $\phi$ adjacent to the lens boundary as a constant, we have neglected any role that might be played by the rearrangement of soil particles. A related issue is our assumption that a new lens is initiated immediately once $p_p$ reaches zero, thereby neglecting the dynamics involved in separating the soil particles at $z_n$. Partial justification for using a constant $\phi$ is provided by the observation that the scaled pressure between soil particles is entirely compressive prior to the predicted initiation of a new lens, as shown in figure 7. We recognize, however, that intermolecular interactions between the soil particles themselves can lead to finite particle separations that change with variations in $p_p$, and these interparticle forces might gain particular importance as $p_p$ tends to zero. If the packing arrangement of soil particles beneath the warmest extent of the pore ice $z_f$ changes significantly, it is possible that ice may nucleate in larger pores that are disconnected from the base of the growing lens. In addition, the presence of soluble impurities may strongly influence the heaving behaviour in both laboratory and natural environments (e.g. Wettlaufer 1999*b*; Watanabe & Mizoguchi 2002). While such complications are beyond the scope of the current work, the model we have presented here provides a framework for further investigation of these issues.

This work has benefited from critical discussions and correspondence with Greg Dash, Andrew Fowler, Bernard Hallet, Howard Stone, Oscar Vilches, Larry Wilen and an anonymous referee. This research is supported by the National Science Foundation, under Grant No. OPP9908945, and by Yale University.

## Appendix. Ice saturation and permeability

For $T < T_m$, interfacial premelting causes liquid to coat particle surfaces in thin films (e.g. see figure 1). The Gibbs–Thomson effect leads to the formation of melt conduits, similar in cross-section to the plateau borders of a foam, near the particle contacts and other regions where the curvature of the ice–liquid interface is high. The liquid fractions in both the films and the conduits decrease as $\Delta T \equiv T_m - T$ increases – the former as $\Delta T^{-1/\nu}$, where $\nu \geqslant 1$ depends on the type of intermolecular interactions that dominate (e.g. Wettlaufer *et al.* 1996); the latter as $\Delta T^{-2}$. Cahn, Dash & Fu (1992) calculated the liquid content in porous media composed of idealized packings of mono-dispersed spheres for the case where $\nu = 3$. Their predictions were consistent

with results from freezing experiments conducted in polystyrene and graphitized carbon-black powders. They found that the liquid fraction is dominated by the melt conduits when $\Delta T \lesssim 10(T_m - T_f)$ where $T_f$ is the coldest temperature at which the pores are completely filled with liquid (i.e. $S_s = 0$). In this thermal regime we can neglect the volume of liquid contained within the premelted films and assume that the liquid fraction varies as $\Delta T^{-2}$. We treat the case where the ice saturation level is continuous across the boundary where ice first begins to invade the pore space so that $S_s = 0$ for $z < z_f$ and

$$S_s = 1 - \left(\frac{z_f}{z}\right)^2 \quad \text{for} \quad z \geqslant z_f, \tag{A 1}$$

where $z_f$ is given by equation (3.1). Note that although the pressure dependence of $T_m$ can be included in the above development, this effect is negligible, as discussed following equation (2.1). Equation (A 1) is used instead of the function describing the unfrozen water content $W(T)$ employed by O'Neill & Miller (1985).

The manner in which the permeability of the partially frozen soil decreases as the pores fill with ice depends on the geometry of the pathways through which the liquid flows. Since we expect the Gibbs–Thomson effect to be responsible for the presence of most of the liquid, we model the permeability by considering the flow through a randomly oriented set of conduits with radii $r$ proportional to the interfacial curvature, which varies as $\Delta T^{-1}$. For this conceptual model of a porous network, the permeability is proportional to the product of the liquid fraction and the square of the conduit radii (e.g. Phillips 1991, p. 33). We define the permeability of the fluid-saturated soil as $k(z \leqslant z_f) = k_0$ and assume that $k$ is continuous across $z_f$ so that

$$k = k_0 (1 - S_s) r^2 = k_0 \left(\frac{z_f}{z}\right)^4 \quad \text{for} \quad z \geqslant z_f. \tag{A 2}$$

In some porous media, the conduits will only connect through the films so that the overall permeability will be significantly affected by the flow resistance through both. Indeed, empirical determinations of both $S_s$ and $k$ might improve quantitative comparisons between the model predictions and experiments. For our current purposes, however, we retain these simple formulations to focus better on the essential features of frost-heave phenomena common to all porous materials rather than the heave characteristics of any particular soil. Using equations (A 1) and (A 2) in equation (3.11) for the heave rate gives

$$v_l = \frac{1 - p_o + (1 - \phi)(\xi_l - 1) + \phi\left(1 - \xi_l^{-1}\right)}{1 - \xi_h + \frac{1}{5}(1 - \phi)^2\left(\xi_l^5 - 1\right) + \frac{2}{3}\phi(1 - \phi)\left(\xi_l^3 - 1\right) + \phi^2(\xi_l - 1)}. \tag{A 3}$$

## REFERENCES


Baker, M. B. & Dash, J. G. 1989 Charge transfer in thunderstorms and the surface melting of ice. *J. Cryst. Growth* **97**, 770–776.

Batchelor, G. K. 1967 *An Introduction to Fluid Dynamics*. Cambridge University Press.

Beskow, G. 1935 *Soil Freezing and Frost Heaving with Special Application to Roads and Railroads*. The Swedish Geological Society, C, no. 375, Year Book no. 3 (translated by J. O. Osterberg). Technological Institute, Northwestern University. Reprinted in: *Historical Perspectives in Frost Heave Research* (ed. P. B. Black & M. J. Hardenberg). CRREL Special Report 91-23, pp. 37–157.

Cahn, J. W., Dash, J. G. & Fu, H. 1992 Theory of ice premelting in monosized powders. *J. Cryst. Growth* **123**, 101–108.

Chernov, A. A., Temkin, D. E. & Mel'nikova, A. M. 1976 Theory of the capture of solid inclusions during the growth of crystals from the melt. *Sov. Phys. Crystallogr.* **21**, 369–373.

Dash, J. G. 1989 Thermomolecular pressure in surface melting: motivation for frost heave. *Science* **246**, 1591–1593.

Dash, J. G., Fu, H. Y. & Wettlaufer, J. S. 1995 The premelting of ice and its environmental consequences. *Rep. Prog. Phys.* **58**, 115–167.

Derjaguin, B. V. & Churaev, N. V. 1978 The theory of frost heaving. *J. Colloid Interface Sci.* **67**, 391–396.

Everett, D. H. 1961 The thermodynamics of frost damage to porous solids. *Trans. Faraday Soc.* **57**, 1541–1551.

Fowler, A. C. 1989 Secondary frost heave in freezing soils. *SIAM J. Appl. Maths* **49**, 991–1008.

Fowler, A. C. 1997 *Mathematical Models in the Applied Sciences*. Cambridge University Press.

de Gennes, P. G. 1985 Wetting: statics and dynamics. *Rev. Mod. Phys.* **57**, 827–63.

Gilpin, R. R. 1979 A model of the "liquid-like" layer between ice and a substrate with applications to wire regelation and particle migration. *J. Colloid Interface Sci.* **68**, 235–251.

Gilpin, R. R. 1980 A model for the prediction of ice lensing and frost heave in soils. *Water Resour. Res.* **16**, 918–930.

Mizusaki, T. & Hiroi, M. 1995 Frost heave in He. *Physica* B **210**, 403–410.

Mutou, Y., Watanabe, K., Ishizaki, T. & Mizoguchi, M. 1998 Microscopic observation of ice lensing and frost heave in glass beads. In *Proc. Seventh Intl. Conf. on Permafrost, June 23–27, 1998, Yellowknife, Canada* (ed. A. G. Lewkowicz & M. Allard), pp. 283–287. Universite Laval, Montreal, Canada.

O'Neill, K. & Miller, R. D. 1985 Exploration of a rigid ice model of frost heave. *Water Resour. Res.* **21**, 281–296.

Phillips, O. M. 1991 *Flow and Reactions in Permeable Rocks*. Cambridge University Press.

Raviv, U. & Klein, J. 2002 Fluidity of bound hydrate layers. *Science* **297**, 1540–1543.

Rempel, A. W., Wettlaufer, J. S. & Worster, M. G. 2001 Interfacial premelting and the thermomolecular force: thermodynamic buoyancy. *Phys. Rev. Lett.* **87**, 088501.

Rempel, A. W. & Worster, M. G. 1999 The interaction between a particle and an advancing solidification front. *J. Cryst. Growth* **205**, 427–440.

Rempel, A. W. & Worster, M. G. 2001 Particle trapping at an advancing solidification front with interfacial-curvature effects. *J. Cryst. Growth* **223**, 420–432.

Sadtchenko, V. & Ewing, G. E. 2002 Interfacial melting of thin ice films: An infrared study. *J. Chem. Phys.* **116**, 4686–4697.

Schick, M. 1990 Introduction to wetting phenomena. In *Les Houches, Session XLVIII, 1988 – Liquids at Interfaces* (ed. J. Charvolin, J. F. Joanny, & J. Zinn-Justin), pp. 415–497. Elsevier.

Taber, S. 1929 Frost heaving. *J. Geol.* **37**, 428–461.

Taber, S. 1930 The mechanics of frost heaving. *J. Geol.* **38**, 303–317.

Vignes-Adler, M. 1977 On the origin of the water aspiration in a freezing dispersed medium. *J. Colloid Interface Sci.* **60**, 162–171.

Watanabe, K. & Mizoguchi, M. 2000 Ice configuration near a growing ice lens in a freezing porous medium consisting of micro glass particles. *J. Cryst. Growth* **213**, 135–140.

Watanabe, K. & Mizoguchi, M. 2002 Amount of unfrozen water in frozen porous media saturated with solution. *Cold Reg. Sci. Tech.* **34**, 103–110.

Wettlaufer, J. S. 1999*a* Ice surfaces: Macroscopic effects of microscopic structure *Phil. Trans. R. Soc. Lond.* A **357**, 3403–3425.

Wettlaufer, J. S. 1999*b* Impurity effects in the premelting of ice. *Phys. Rev. Lett.* **82**, 2516–1519.

Wettlaufer, J. S. & Worster, M. G. 1995 Dynamics of premelted films: Frost heave in a capillary. *Phys. Rev.* E **51**, 4679–4689.

Wettlaufer, J. S., Worster, M. G., Wilen, L. A. & Dash, J. G. 1996 A theory of premelting dynamics for all power law forces. *Phys. Rev. Lett.* **76**, 3602–3605.

Wilen, L. A. & Dash, J. G. 1995 Frost heave dynamics at a single-crystal interface. *Phys. Rev. Lett.* **74**, 5076–5079.

Worster, M. G. & Wettlaufer, J. S. 1999 The fluid mechanics of premelted liquid films. In *Fluid Dynamics at Interfaces* (ed. W. Shyy & R. Narayanan), pp. 339–351. Cambridge University Press.

Zhu, D.-M., Vilches, O. E., Dash, J. G., Sing, B. & Wettlaufer, J. S. 2000 Frost heave in argon. *Phys. Rev. Lett.* **85**, 4908–4911.